

Genetic Algorithm-Based Beam Widening for Transmitting Multi-Feed RIS-Assisted Systems

Hanlin Guan, Mahmoud Naamani, and Hmaied Shaiek

Abstract – Reconfigurable intelligent surfaces (RISs) have emerged as a promising technology for improving the performance of wireless communication systems. Although single-feed RIS has shown great potential in coverage extension, its beamforming capability is often limited. In this paper, we investigate the potential of quad-feed transmitting RIS (T-RIS) to enhance beam widening in wireless communication systems using genetic algorithms. Using multiple feed points, the proposed 4-feed T-RIS architecture significantly enhances the beamwidth and coverage. Simulation results show that the 4-feed T-RIS significantly improves half-power beamwidth while maintaining a low side-lobe level. The proposed method presents a promising solution for improving wireless coverage in challenging environments.

1. Introduction

Reconfigurable intelligent surfaces (RIS) have demonstrated their potential to enhance spectral efficiency and reduce energy consumption in wireless networks by actively controlling the propagation environment. These surfaces are considered essential for improving signal coverage in millimeter-wave (mmWave) multiple-input multiple-output (MIMO) communication systems [1]. Integrating an RIS into a MIMO system imposes several challenges. The potential gain of the RIS relies heavily on the design of the beams, which, in turn, depends on the availability of accurate channel state information. Knowledge of the user's location is required to perform beamforming for a specific user, which can be obtained using a dedicated channel estimation technique. In [2], the authors proposed a two-stage iterative re-weighted approach for estimating the channel in a downlink RIS-aided mmWave MIMO system. Furthermore, in [3], the authors investigated channel estimation for RIS-aided mmWave MIMO systems, using atomic norm minimization to estimate the channel parameters.

Optimizing the beams improves channel estimation accuracy by minimizing the estimation error and enhances system performance by maximizing the achievable data rate.

According to our previous research on single-feed T-RIS scenarios [4], the genetic algorithm (GA)-based

mask shape optimization method performs well. However, we found that when the target half-power beamwidth (HPBW) is large, performance metrics such as side-lobe level (SLL) cannot meet the requirements of realistic scenes. Therefore, this paper builds on the foundation of previous research to expand the approach from the direction of 4-feed T-RIS, which is dedicated to obtaining wider HPBW while keeping low SLL using a GA-based optimization method. In addition to wider HPBW, multi-feed T-RIS paves the way for multi-user systems, enabling simultaneous communication with multiple users. However, for practical applications, a moderate number of feeds should be considered, as many feeds would result in more complex systems [5]. The paper is organized as follows: Section II introduces the system model and basic concepts, Section III explains the formulation of the optimization problem, Section IV gives the simulation results, and Section V concludes the paper.

2. System Model

This paper presents a generic RIS-assisted multi-input-single-output (MISO) wireless communication system operating in transmitting array mode with 4-feeders elements. The system architecture is illustrated in Figure 1. First, we consider an $M \times N$ square RIS configuration. The RIS is positioned in the x-y plane of the Cartesian coordinate system, with its geometric center coinciding with the coordinate origin.

Each unit cell (UC) has dimensions d_x along the x-axis and d_y along the y-axis, where $d_x = d_y = \lambda/2$ with λ denoting the operating wavelength. The physical area of each UC is given by $A_{\text{phy}} = d_x \times d_y$. The maximum aperture size of the RIS is characterized by parameter D , which is expressed as $D = \max(M \times d_x, N \times d_y)$. The proposed T-RIS configuration employs 4-feed horn antennas, partitioning the RIS into four equal subarrays. Each feeder is positioned at the centroid of its corresponding subarray in the x-y plane, positioned along the negative Z-axis at a focal distance F .

The power radiation pattern of the p^{th} feeder is given by $F^{\text{tx},p}(\theta_{m,n}^{\text{tx},p}) = 2(4 + 1)\cos^4(\theta_{m,n}^{\text{tx},p})$. Each UC incorporates phase shifts connected to the Tx radiating elements, modeled as uniform apertures with transmission power radiation patterns expressed as $F^{\text{t},p}(\theta_{m,n}^{\text{t},p}) = \pi\cos(\theta_{m,n}^{\text{t},p})$ for the p^{th} feeder. Here, $\theta_{m,n}^{\text{t},p}$ denotes the elevation angle between the $(m, n)^{\text{th}}$ UC and the p^{th} feeder. As shown in Figure 1, $\theta_{m,n}^{\text{t},p}$ is equivalent to $\theta_{m,n}^{\text{tx},p}$ in this system model.

Manuscript received 18 December 2024.

Hanlin Guan, Mahmoud Naamani, and Hmaied Shaiek are with Conservatoire national des arts et métiers: Conservatoire National des Arts et Metiers Paris, FRANCE; e-mail: hanlin.guan.auditeur@lecnam.net, mahmoud.naamani@lecnam.net, hmaied.shaiek@lecnam.net.

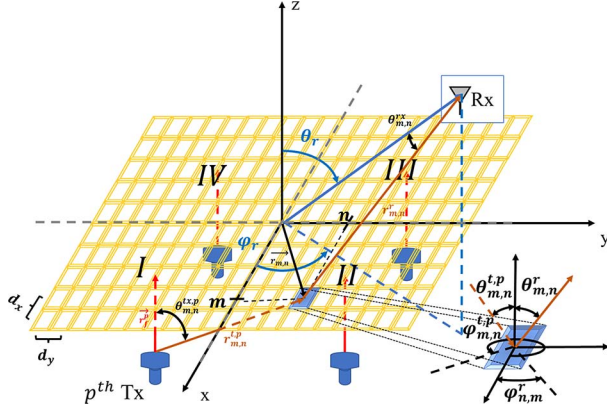


Figure 1. T-RIS system model with 4 feeds.

2.1 Electric Field

This paper exclusively considers the far-field transmission scenario, where the receiver's distance from the RIS center exceeds the Rayleigh distance defined as $L = 2D^2/\lambda$, marking the boundary between far-field and near-field regions. We adopt the following key assumptions: (1) The peak radiation direction of the Rx antenna is aligned with the RIS center, while each Tx antenna beam is directed toward its respective subarray center; (2) All unit cells share uniform amplitude transmission coefficients with distinct phase shifts $\phi_{m,n}$. To enhance computational efficiency, we employ a two-dimensional inverse fast Fourier transform implementation that simultaneously maps spatial directions (θ_r, φ_r) to angular coordinates. The resultant electric field expression for the 4-feed transmitting array configuration in the far-field (u, v) coordinate system is formulated as:

$$E(u, v) = C \sum_{p=1}^4 \text{IFFT} \left[\frac{\sqrt{F^{\text{Tx},p}(\theta_{m,n}^{\text{Tx},p}) \times F^{\text{L},p}(\theta_{m,n}^{\text{L},p})}}{\|\vec{r}_{m,n}^p - \vec{r}_f^p\|} \right] \times e^{j\phi_{m,n} - jk\|\vec{r}_{m,n}^p - \vec{r}_f^p\|} \quad (1)$$

where the normalization factor $C = (1 - u^2 - v^2)^{1/4} MN$, with spatial frequency coordinates defined as $u = \sin(\theta_r)\cos(\varphi_r) = \frac{2\pi}{N_x^{\text{FFT}}d_x}p$ and $v = \sin(\theta_r)\sin(\varphi_r) = \frac{2\pi}{N_y^{\text{FFT}}d_y}q$. The indices span $p = -\frac{N_x^{\text{FFT}}-1}{2}, \dots, \frac{N_x^{\text{FFT}}-1}{2}$ and $q = -\frac{N_y^{\text{FFT}}-1}{2}, \dots, \frac{N_y^{\text{FFT}}-1}{2}$. Here, \vec{r}_f^p denotes the position vector from the p^{th} transmitter to its associated subarray center, $\vec{r}_{m,n}^p$ represents the vector from subarray center to the $(m, n)^{\text{th}}$ UC, and $e^{j\phi_{m,n}}$ governs the phase control of the $(m, n)^{\text{th}}$ UC. The directivity

formulation in (u, v) coordinates follows the established relationship [8]:

$$D_0 = \frac{4\pi|E(u_r, v_r)|^2}{\int_{-1}^1 \int_{-1}^1 \frac{|E(u, v)|^2}{\sqrt{1-u^2-v^2}} du dv} \quad (2)$$

3. Optimization Problems

Consistent with our prior investigations [4], this work maintains the genetic algorithm GA-based methodology from [6] for optimizing UC phase matrices to achieve radiation patterns with SLL under enhanced HPBW constraints. This phase matrix computation is formulated as an optimization problem to minimize the discrepancy between computed and ideal radiation patterns. Focusing on SLL and HPBW metrics, the GA objective function follows [6]:

$$F_{obj} = \sum_{(u,v) \in S_L} \left(\frac{\hat{E}(u, v) - M_L(u, v)}{|S_L|} \right)^2 + \sum_{(u,v) \in S_U} \left(\frac{\hat{E}(u, v) - M_U(u, v)}{|S_U|} \right)^2 \quad (3)$$

where $S_L = \{(u, v) | \hat{E}(u, v) < M_L(u, v)\}$ and $S_U = \{(u, v) | \hat{E}(u, v) > M_U(u, v)\}$. Here, \hat{E} denotes the normalized radiation pattern, while M_L and M_U represent lower/upper masks containing HPBW and SLL specifications, respectively. The former governs HPBW control while the latter suppresses SLL, with $|\cdot|$ indicating set cardinality.

Our previous analysis [4] demonstrated comparable performance between circular and elliptical masks. However, elliptical masks exhibited superior HPBW regulation, SLL reduction, and directivity maintenance, particularly at large beam steering angles. Consequently, we exclusively employ elliptical masks for beam widening in 4-feed T-RIS configurations. The elliptical mask formulations from [4] are as follows:

$$M_L(u, v) = \begin{cases} \min(\hat{E}(u, v)) & \text{for } \mathcal{E}_L(u, v; \Theta_{hp}) > 1 \\ -3 & \text{for } \mathcal{E}_L(u, v; \Theta_{hp}) \leq 1 \end{cases} \quad (4)$$

$$M_U(u, v) = \begin{cases} \tau & \text{for } \mathcal{E}_U(u, v; \Theta_{fn}) > 1 \\ 0 & \text{for } \mathcal{E}_U(u, v; \Theta_{fn}) \leq 1 \end{cases} \quad (5)$$

where $\mathcal{E}(u, v; \Theta) = \frac{((u-u_0)\cos\alpha + (v-v_0)\sin\alpha)^2}{\sin^2\frac{\Theta}{2}} + \frac{((u-u_0)\sin\alpha - (v-v_0)\cos\alpha)^2}{\sin^2\frac{\Theta}{2}\cos^2\theta_r}$ with $\alpha = \varphi_r + \frac{\pi}{2}$. Main beam direction (θ_r, φ_r) in spherical coordinates (Figure 1) corresponds to angular coordinates (u_0, v_0) , while τ specifies target SLL. Parameters Θ_{hp} and Θ_{fn} control HPBW and first-null beamwidth, respectively.

Table 1. Beamwidths, SLLs, and directivity generated with different steering angles before and after optimization

Before optimization (4 feed)				$\Theta^t = 20^\circ$ (1 feed)		
θ_r	$\Theta(^{\circ}) : (\theta, \phi)$	SLL(dB)	D (dBi)	$\Theta(^{\circ}) : (\theta, \phi)$	SLL(dB)	D (dBi)
0°	(11.13, 11.13)	-14.37	21.38	(22.32, 22.65)	-4.11	15.55
20°	(11.51, 11.25)	-10.98	21.14	(25.73, 19.88)	-2.59	14.21
40°	(14.23, 11.25)	-11.83	20.17	/	/	/
60°	(20.13, 11.13)	-9.55	18.54	/	/	/
$\Theta^t = 20^\circ$ (4 feed)				$\Theta^t = 25^\circ$ (4 feed)		
0°	(19.95, 20.22)	-11.93	17.36	(24.95, 24.81)	-8.19	16.29
20°	(20.85, 20.04)	-10.94	17.07	(24.93, 24.90)	-10.02	15.99
40°	(20.33, 20.47)	-10.58	16.82	(25.12, 25.35)	-7.48	15.60
60°	(20.45, 19.93)	-6.85	15.85	(25.68, 25.43)	-5.04	14.44

4. Simulation Results

This subsection demonstrates key simulation results for the 4-feed T-RIS configuration. The GA parameters align with our previous 1-feed scenario studies [4]. Our simulations employ a square $M \times N = 20 \times 20$ RIS operating at $f_c = 26$ GHz with wavelength $\lambda = c/f_c = 11.53 \times 10^{-3}$ m. Following [7], we

set the optimal F/D ratio to 0.26 for this array configuration. The optimization framework, implemented in Python using pymoo library, minimizes the cost function (3) with a fixed random seed of 1.

The UNSGA3 algorithm configuration includes the following: population size $W = 1000$, evolving through 400 generations with Latin Hypercube Sampling initialization. Genetic operators employ binomial crossover ($P_c = 0.9$) and Gaussian mutation ($P_m = 0.1$), complemented by duplicate elimination and elitism (value = 6). Phase matrix optimization begins with $W = 1000$ candidates of 20×20 float matrices ($\phi \in [0, \pi]$), using reference directions (“energy”, 1, 1000).

Table 1 shows the 1-bit quantized beamwidths, SLLs, and directivities for different steering angles in the 4-feed T-RIS configuration before and after optimization, comparing the two following cases: $\Theta^t = \Theta_{hp} = 20^\circ$ & $\Theta_{fn} = 25^\circ$ and $\Theta^t = \Theta_{hp} = 25^\circ$ & $\Theta_{fn} = 31^\circ$. Optimized results for the 1-feed configuration with $\Theta^t = 20^\circ$ are also included. The 1-feed configuration demonstrates limited effectiveness for large steering angles ($\theta_r = 40^\circ, 60^\circ$)

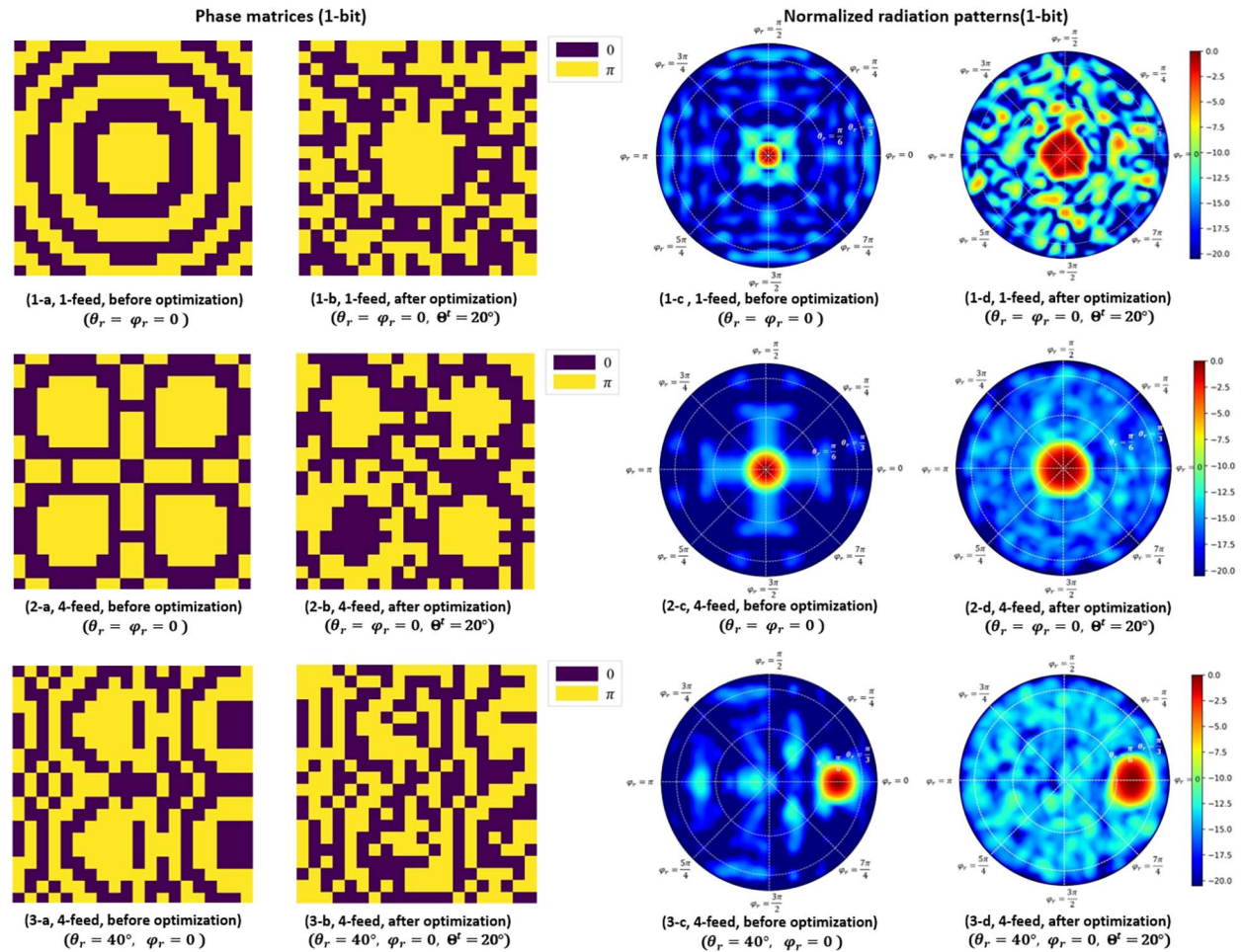


Figure 2. Some results of 1-bit phase matrices and normalized radiation patterns for 1 feed and 4 feed (see the subheadings in the figure for more details).

under $\Theta^f = 20^\circ$ conditions, with unsatisfactory SLLs and directivities even at $\theta_r = 0^\circ, 20^\circ$. For all optimized 4-feed cases, the obtained HPBW $\Theta : (\theta, \phi)$ successfully meet the preset targets ($\Theta^f = 20^\circ$ and 25° respectively). With increasing steering angle θ_r , the SLL shows an ascending trend under both $\Theta^f = 20^\circ$ and 25° conditions. Additionally, beam directivity exhibits consistent reduction as HPBW widens across all steering angles.

Figure 2 presents comparative analyses of 1-bit phase matrices and normalized radiation patterns under different configurations. The first subplot displays (1-a) and (1-c) preoptimization results for 1-feed configuration with $\theta_r = 0^\circ, \varphi_r = 0^\circ$; (1-b) and (1-d) GA-optimized results using $\Theta^f = 20^\circ$ and $\tau = -20$ dB. The second subplot (2-a)-(2-d) shows 4-feed configuration results with $\tau = -18$ dB. The final subplot (3-a)-(3-d) demonstrates 4-feed performance under $\theta_r = 40^\circ, \varphi_r = 0^\circ, \Theta^f = 20^\circ$, and $\tau = -15$ dB.

The visual comparisons reveal the following three key observations: First, optimized cases exhibit significantly expanded HPBW at the cost of elevated sidelobe levels. Second, comparative analysis between (1-d) and (2-d) confirms the 4-feed configuration's superior sidelobe suppression capability—achieving lower SLL ($\tau = -18$ dB vs. -20 dB) while maintaining identical $\Theta^f = 20^\circ$ HPBW targets. Third, the 4-feed system demonstrates fundamentally improved sidelobe characteristics throughout the radiation pattern.

Extended analysis of 4-feed results demonstrates two angular dependencies. As θ_r increases from 0° to 40° , we observe progressive SLL degradation (from -18 dB to -15 dB) accompanied by directivity reduction—consistent with Table 1 findings. Simultaneously, the main beam undergoes shape transformation from circular to elliptical in the (u, v) plane. This geometric distortion stems from diverging HPBW values in elevation versus azimuthal planes at large steering angles [4], fundamentally justifying our elliptical mask optimization approach. Crucially, the 4-feed architecture demonstrates effective SLL containment (15 dB degradation vs. 1-feed's 20 dB) while maintaining prescribed HPBW expansion.

5. Conclusion

Building upon our prior investigations of 1-feed T-RIS configurations [4], this work generalizes the methodology to multifeed MISO scenarios through 4-feed T-RIS beamwidth enhancement. The GA-driven elliptical mask optimization technique demonstrates comparable

effectiveness in 4-feed configurations, maintaining its core operational principles from previous implementations. Numerical simulations confirm the capability of the 4-feed T-RIS to achieve enhanced HPBW while containing SLL degradation. Future research directions will investigate channel state information estimation strategies for the developed beam patterns in multi-user MISO environments.

6. Acknowledgment

This work has been done in context of the MESANGES Project ANR-20-CE25-0016-01.

7. References

1. L. Jiao, P. Wang, A. Alipour-Fanid, H. Zeng, and K. Zeng, "Enabling Efficient Blockage-Aware Handover in RIS-Assisted mmWave Cellular Networks," *IEEE Transactions on Wireless Communications*, **21**, 4, 2021, pp. 2243-2257.
2. J. He, M. Leinonen, H. Wymeersch, and M. Juntti, "Channel Estimation for RIS-Aided mmWave MIMO Systems," *GLOBECOM 2020-2020 IEEE Global Communications Conference*, Taipei, Taiwan, December 7–11, 2020.
3. J. He, Jiguang, H. Wymeersch, and M. Juntti, "Channel Estimation for RIS-Aided mmWave MIMO Systems Via Atomic Norm Minimization," *IEEE Transactions on Wireless Communications*, **20**, 9, 2021, pp. 5786-5797.
4. H. Guan, M. A. Hajj, V. Guillet, and H. Shaiek, "Enhanced Beam Widening Approach for RIS-Assisted Wireless Communication Systems," *2024 4th URSI Atlantic Radio Science Meeting (AT-RASC)*, Meloneras, Spain, May 19–24, 2024.
5. A. Clemente, L. Dussopt, R. Sauleau, P. Potier, P. Pouliguen, "Focal Distance Reduction of Transmit-Array Antennas Using Multiple Feeds," *IEEE Antennas and Wireless Propagation Letters*, **11**, November, 2012, pp. 1311-1314.
6. M. Al Hajj, K. Tahkoubit, H. Shaiek, V. Guillet, and D. L. Ruyet, "On Beam Widening for RIS-Assisted Communications Using Genetic Algorithms," *2023 Joint European Conference on Networks and Communications and 6G Summit (EuCNC/6G Summit)*, Gothenburg, Sweden, June 6–9, 2023.
7. D. Demmer, F. Foglia Manzillo, S. Gharbieh, M. Śmierchalski, et al., "Hybrid Precoding Applied to Multi-Beam Transmitting Reconfigurable Intelligent Surfaces (T-RIS)," *Electronics*, **12**, 5, 2023, p. 1162.
8. W. P. M. N. Keizer, "Synthesis of Scan- and Frequency-Invariant Low-Sidelobe Tapers for Planar Array Antennas," *IEEE Transactions on Antennas and Propagation*, **64**, 8, 2016, pp. 3703-3707.